Nanoscale

PAPER

View Article Online
View Journal | View Issue

Cite this: *Nanoscale*, 2016, **8**, 7723

Self-healing gold mirrors and filters at liquid–liquid interfaces†

Evgeny Smirnov,[a] Pekka Peljo,[a] Micheál D. Scanlon,[b] Frederic Gumy[a] and Hubert H. Girault*[a]

The optical and morphological properties of lustrous metal self-healing liquid-like nanofilms were systematically studied for different applications (*e.g.*, optical mirrors or filters). These nanofilms were formed by a one-step self-assembly methodology of gold nanoparticles (AuNPs) at immiscible water–oil interfaces, previously reported by our group. We investigated a host of experimental variables and herein report their influence on the optical properties of nanofilms: AuNP mean diameter, interfacial AuNP surface coverage, nature of the organic solvent, and nature of the lipophilic organic molecule that caps the AuNPs in the interfacial nanofilm. To probe the interfacial gold nanofilms we used *in situ* (UV-vis-NIR spectroscopy and optical microscopy) as well as *ex situ* (SEM and TEM of interfacial gold nanofilms transferred to silicon substrates) techniques. The interfacial AuNP surface coverage strongly influenced the morphology of the interfacial nanofilms, and in turn their maximum reflectance and absorbance. We observed three distinct morphological regimes; (i) smooth 2D monolayers of "floating islands" of AuNPs at low surface coverages, (ii) a mixed 2D/3D regime with the beginnings of 3D nanostructures consisting of small piles of adsorbed AuNPs even under sub-full-monolayer conditions and, finally, (iii) a 3D regime characterised by the 2D full-monolayer being covered in significant piles of adsorbed AuNPs. A maximal value of reflectance reached 58% in comparison with a solid gold mirror, when 38 nm mean diameter AuNPs were used at a water–nitrobenzene interface. Meanwhile, interfacial gold nanofilms prepared with 12 nm mean diameter AuNPs exhibited the highest extinction intensities at *ca.* 690 nm and absorbance around 90% of the incident light, making them an attractive candidate for filtering applications. Furthermore, the interparticle spacing, and resulting interparticle plasmon coupling derived optical properties, varied significantly on replacing tetrathiafulvalene with neocuproine as the AuNP capping ligand in the nanofilm. These interfacial nanofilms formed with neocuproine and 38 nm mean diameter AuNPs, at monolayer surface coverages and above, were black due to aggregation and broadband absorbance.

Received 15th January 2016,
Accepted 6th March 2016

DOI: 10.1039/c6nr00371k

www.rsc.org/nanoscale

Introduction

Currently, mirrors and filters are produced industrially by thin film technology.[1] The manufacturing process is technically challenging, requiring large metal evaporation chambers operating under vacuum conditions and clean-room environments. A proposed industrially viable alternative approach towards the development of thin film optical technology, potentially circumventing the need for such stringent, complex and costly process environments, is the controlled large-scale self-assembly of nanoparticles (NPs) with tunable optical responses on various substrates[2,3] and interfaces.[4–8] In this regard, metallic NPs, which possess Localized Surface Plasmon Resonance (LSPR) in the visible or near-infrared (NIR) range of the electromagnetic spectrum, open new avenues towards the development of scalable, low cost mirrors and filters.[9–12] The optical responses of the latter are tunable (i) by the intrinsic properties of the individual NPs, with the optical properties of noble metallic NPs such as silver (AgNPs) or gold (AuNPs) dependent on their size and shapes, and (ii) by the packing arrangements and spacing between individual NPs in the assemblies.[7,13–15]

There are two main disadvantages of self-assembly processes at liquid–solid interfaces: expansion across films on large-scales, and poor reproducibility between process batches.

[a]*Laboratoire d'Electrochimie Physique et Analytique, Ecole Polytechnique Fédérale de Lausanne, Rue de l'Industrie 17, CH-1951 Sion, Switzerland.*
E-mail: hubert.girault@epfl.ch
[b]*Department of Chemistry, the Tyndall National Institute and the Analytical & Biological Chemistry Research Facility (ABCRF), University College Cork, Cork, Ireland*

†Electronic supplementary information (ESI) available: Interfacial tension measurements for various water–organic solvent systems, step-by-step optical microscopy and SEM characterization of the obtained film, optical photographs of all tested solvents and molecules, and influence of the interfacial tension on optical responses of AuNPs assemblies. See DOI: 10.1039/c6nr00371k

In contrast, liquid–liquid interfaces are inherently defect-free and, furthermore, both mechanically flexible, and possessing self-recovery characteristics.[16–20] Thus, liquid–liquid interfaces represent an ideal system to perform self-assembly of a panoply of species, ranging from molecules[21,22] to NPs[14,23,24] to microparticles,[25] into two-dimensional ordered films. The latter for NPs has been recently reviewed in detail.[26] Crucially for the production of optical technology, NP films (nanofilm) at liquid–liquid interfaces remain stable for time periods ranging from months to years.[24,27]

Since Yogev and Efrima[28] first described the formation of metal liquid-like films upon the reduction of silver salts at liquid–liquid interfaces, many other methods have been introduced to form such nanofilms, *e.g.* addition of ethanol or methanol to the interfacial region,[23,29,30] precise injection of colloidal AuNP solutions prepared in methanol at water–organic solvent interfaces,[31] use of salts,[32] solvent evaporation,[33] covalent bonding[14,34,35] and self-assembly provided by electrostatic interactions.[36–38] Applications of these self-assembled nanofilms include filters, mirrors[5,39] or smart mirrors,[40] substrates for Surface Enhanced Raman Spectroscopy (SERS),[41–44] and enhancement of non-linear Second Harmonic Generation (SHG) optical responses.[45–47] Finally, these nanofilms were used to achieve electrocatalysis at electrically polarized liquid–liquid interfaces.[48,49]

Recently, our group introduced a facile biphasic method to self-assemble nanofilms of AuNPs at water–1,2-dichloroethane (DCE) interfaces with controllable interfacial AuNP surface coverages (θ_{int}^{AuNP}).[24] Briefly, a lipophilic species (tetrathiafulvalene; TTF) was present in the DCE phase and which came into contact with an aqueous solution of citrate-stabilized AuNPs. Upon vigorous mechanical shaking, TTF displaced the citrate ligands from the surface of the AuNPs and, in turn, underwent Fermi-level equilibration with the AuNPs becoming oxidized to $TTF^{+\bullet}$ or possibly, but less likely, to TTF^{2+}. These $TTF^{+\bullet}$ coated AuNPs were entrapped at the liquid–liquid interface upon cessation of shaking. We postulate that the $TTF^{+\bullet}$ molecules act both as a "glue", holding the AuNPs together due to π–π-interactions between TTF molecules, and as a "lubricant" permitting the reproducible self-healing behavior of the interfacial gold nanofilm after substantial perturbations, such as vigorous mechanical shaking. In this context, self-healing means that the gold nanofilm retains its metallic lustrous properties after substantial perturbations. Thus, the TTF molecule prevents irreversible AuNP aggregation at the liquid–liquid interface which would destroy the optical properties of the lustrous nanofilm.[24] Finally, the optical extinction spectra and observed visual appearance of the interfacial AuNP assemblies varied substantially depending on the mean-diameters of the individual AuNPs used to create them.[24]

Herein, we optimized the biphasic experimental conditions to produce self-assembled interfacial gold nanofilms with suitable optical responses for gold mirror or filter applications. To this end, we carried out an *in situ* comparative study of the optical responses (extinction and reflectance) of self-assembled and self-healing interfacial gold nanofilms with (i) different mean diameters (12 and 38 nm Ø), (ii) at various θ_{int}^{AuNP} values, (iii) using several organic solvents to form water–organic interfaces with different interfacial surface tensions ($\gamma_{w/o}$), and (iv) using alternative lipophilic molecules, such as neocuproine (NCP),[7] in the organic droplet instead of TTF.

We identified an optimal value of θ_{int}^{AuNP} at water–DCE interfaces that permitted the maximum coverage of the interface with a 2D monolayer (enhancing reflectance) without the presence of substantial 3D piles of AuNPs. These piles caused the incident light to scatter (diminishing the optical response). We demonstrated that the interparticle spacing between AuNPs in the interfacial nanofilms, and thus their plasmon coupling and optical properties, can be varied significantly by replacing TTF in the organic phase with NCP. Overall, the best optical responses were obtained at water–nitrobenzene interfaces.

Experimental

Chemicals

Tetrachloroauric acid ($HAuCl_4$, 99.9%), neocuproine (NCP) and tetrathiafulvalene (TTF) were received from Aldrich. Citrate trisodium dihydrate ($Na_3C_6H_5O_7{\cdot}2H_2O$), 1,2-dichloroethane (DCE), nitrobenzene (NB), and nitromethane ($MeNO_2$) were purchased from Fluka, whereas α,α,α-trifluorotoluene (TFT) was received from Acros. Silver nitrate ($AgNO_3$) was bought from Chempur and ascorbic acid ($C_6H_8O_6$) from Riedel-de-Haen. All chemicals were used as received without further purification. In all experiments Millipore water (18.2 MΩ cm) was used.

Preparation of aqueous colloidal AuNP solutions and their characterization

Suspensions of AuNPs with various mean diameters were prepared using the seed-mediated growth method.[29] Initially, seed AuNPs were synthesized.[50,51] Briefly, 41.5 mg of $HAuCl_4{\cdot}3H_2O$ was dissolved in 300 mL of deionized water in a round-bottom flask with stirring. This solution was brought to the boiling point and 9 mL of a 1% w/v trisodium citrate solution was injected to form the 12 nm mean diameter AuNPs. Subsequently, to prepare the 38 nm mean diameter AuNPs by seed-mediated growth, 4 mL of 20 mM $HAuCl_4{\cdot}3H_2O$ with 0.4 mL of 10 mM $AgNO_3$ was added to 170 mL of deionized water. To this, under vigorous stirring, 15 mL of the 12 nm Ø AuNP seed solution and 30 mL of 5 mM ascorbic acid solution were added by using a syringe pump in a drop-wise manner with a constant flow rate of 0.5 mL min^{-1}.

The colloidal AuNP solutions were characterized by UV-Vis spectroscopy using a standard Perkin Elmer, Lambda XLS+ spectrophotometer with a 10 mm cell width. By analyzing these spectra as described by Haiss *et al.*[52] information on the mean AuNP diameter and concentration of AuNPs in solution were obtained. Further analysis of the mean AuNP diameter and size distribution was accomplished by dynamic light scattering (DLS) measurements performed with a Nano ZS Zetasizer (Malvern Instruments, UK), with irradiation (λ = 633 nm) from a He–Ne laser, and using Dispersion Technology Software

(DTS). Transmission electron microscopy (TEM) images were obtained using a FEI CM12 (Phillips) transmission electron microscope, operating with a LaB_6 electron source at 120 kV. The size distributions of the AuNPs were estimated by using ImageJ software assuming that the AuNPs were spherical. For each sample 4 to 5 individual images were analysed, collecting information on more than 150 AuNPs.

Preparation of interfacial gold nanofilms and their characterization

Interfacial gold nanofilms were prepared using a biphasic method introduced by our group recently.[24] The typical procedure involves either sonicating or vigorously shaking of a liquid–liquid interface formed by an aqueous colloidal AuNP solution and a droplet of an organic solvent (either DCE, TFT, NB or $MeNO_2$) containing a lipophilic species (either TTF or NCP, typically 1 mM concentrations). Once the color of the agitated solution changed from red to bluish gray, the suspension was left to settle, resulting in an interfacial gold nanofilm covering the entire surface area of the organic droplet. This nanofilm has self-healing nature meaning that the droplet restores its original lustrous properties after being vigorously shaken for several times.

For scanning electron microscopy (SEM) and transmission electron microscopy (TEM) studies only, the interfacial AuNP nanofilms were transferred to a polished silicon substrate or TEM grid, respectively, by carefully dipping the solid support in the organic droplet. These transferred nanofilms were then analyzed further by using a Merlyn (Zeiss, Germany) high-resolution scanning electron microscope (SEM) operating at 3 kV with secondary electron detectors. The interparticle size distributions were estimated by using ImageJ software. For each AuNP sample, 2 to 3 individual HR-TEM images, obtained with the FEI CM12 (Phillips), were analyzed, collecting information on between 50 and 70 interparticle distances.

In situ optical images of interfacial nanofilms in horizontal mode were obtained with a standard BX41 laboratory microscope (Olympus).

UV-Vis-NIR spectra of the interfacial AuNP films were recorded *in situ* at the liquid–liquid interface without transferring the nanofilm to a solid substrate. Two separate configurations were investigated, total transmittance or extinction and total reflectance, as outlined in Scheme 1. The spectra were

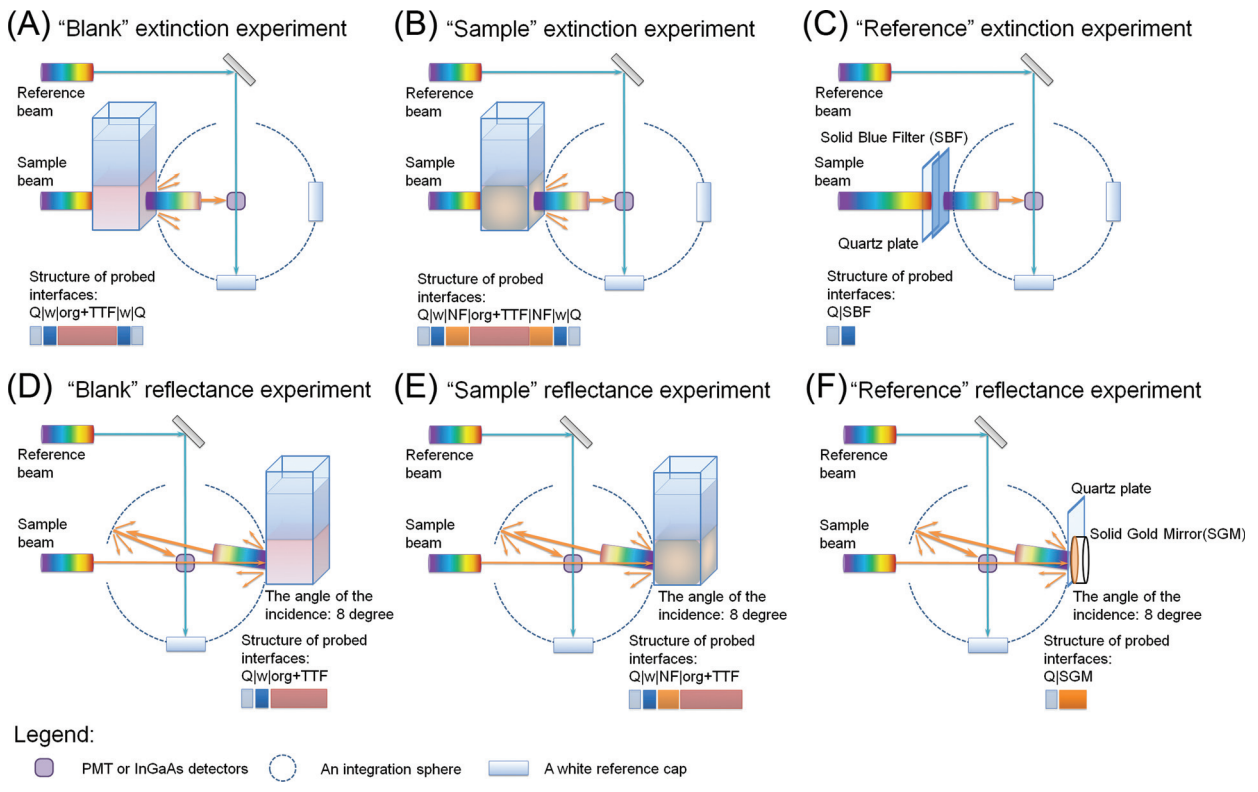

Scheme 1 Extinction and reflectance spectra acquisition for interfacial gold nanofilms: *in situ* UV-Vis-NIR experimental configurations with a white integrating sphere. (A) "Blank" (without the gold nanofilm coating the organic droplet) and (B) "Sample" (with the gold nanofilm coating the organic droplet) extinction spectra were measured through two AuNP films at opposite walls of the quartz cuvette. (C) "Reference" extinction spectra were obtained at a solid blue filter with an additional 2 mm quartz plate in front of it. (D) "Blank" and (E) "Sample" reflectance spectra were obtained at a single interface on one side of the quartz cell. (F) "Reference" reflectance spectra were obtained at a solid gold mirror, separated from the sample-window with a 2 mm quartz plate, and corresponding to 100% reflectance. Q, w, org, NF, SBF and SGM are acronyms for quartz, water, organic solvent, nanofilm of AuNPs, solid blue filter and solid gold mirror, respectively. The colors corresponding to each component in the quartz cell are detailed in the various legends.

obtained using a white integrating sphere, 6 cm in diameter, which was installed inside the PerkinElmer Lambda 950 spectrometer. The sample for the reference beam for all experiments was a white standard SRS-99 (LabSphere).

Extinction and reflectance spectra were recorded for interfacial gold nanofilms prepared at a liquid–liquid interface inside of a quartz cell (QS, Hellma) with a 10 mm light path and 2 mm wall thickness. This cell was fixed either at the entrance to the integrating sphere (Scheme 1A–C) to measure extinction or at the exit (Scheme 1D–F) to obtain reflectance.

The extinction spectra obtained from interfacial 12 nm Ø gold nanofilms were compared with the spectrum of a commercially available blue filter (FGB37S, ThorLabs) (Scheme 1C). All reflectance spectra were compared with the ThorLabs solid gold mirror (PF10-03-M01) separated from the window of the integrating sphere by using a 2 mm thick QS plate with the same thickness as a typical QS cell (Scheme 1F).

In Scheme 1 we depicted how the interfaces were probed for each experimental configuration. To measure the extinction of nanofilms, the light beam has to pass through two gold nanofilms, one at the two opposite sides of the cell, whereas, to record reflectance only one interface can be taken into account. The angle between the incident beam and the beam normal to the surface in the reflectance measurement was 8°. The latter was determined by the diameter of the integrating sphere (6 cm). The bigger the diameter, the closer this angle can be to 0°. However, it cannot achieve exactly 0°, because in this case the reflected beam would leave the sphere through the entrance.

The precise procedure to prepare interfacial gold nanofilms in quartz cuvettes for *in situ* UV-Vis-NIR measurements was as follows. To record the reference spectrum, firstly, 1 ml of an organic solvent (DCE, TFT, NB or $MeNO_2$) containing 0.25 mM of the lipophilic molecule (TTF or NCP) was placed into the quartz cell and a further 2 ml of MilliQ water was added on top. Next once the reference spectra were obtained, the entire aqueous phase was removed and replaced with the required volume of an aqueous colloidal AuNP solution. Then, the cell was shaken vigorously and left for a couple of minutes to allow the emulsion to settle. Finally, the extinction and reflectance spectra were recorded successively as described in Scheme 1 earlier. The overall procedure was repeated step-by-step in the same quartz cell to cover the entire interfacial surface coverage (θ_{int}^{AuNP}) range of interest.

Results and discussion

Mean diameter determination and size distributions of the colloidal AuNP solutions

AuNPs with mean diameters of 12 and 38 nm, respectively, were chosen for the study. The rationale behind the choice of these specific AuNP sizes was that, based on the extinction spectra of interfacial gold nanofilms consisting of 12 and 38 nm Ø AuNPs at water–DCE interfaces reported previously as a function of θ_{int}^{AuNP},[24] we identified the relatively small 12 nm Ø AuNPs as suitable candidates for optical filter applications and the relatively large 38 nm (and above) Ø AuNPs for potential optical mirror applications. In addition, we endeavored to keep the size of the AuNPs below the threshold for electric quadrupole resonance, simplifying the analysis of the spectra. AuNPs possess electric quadrupole and magnetic dipole moments, and different authors have reported various thresholds for electric quadrupole resonance of AuNPs ranging from ~60 or 70[53,54] to ~150 nm Ø.[55]

The AuNPs were synthesized as described in the Experimental section. Both the 12 and 38 nm Ø procedures resulted in mostly spherical AuNPs. The mean diameters were initially determined to be 12 and 38 nm Ø based on the UV-Vis absorbance spectra and considering the maximum of the SPR-peak intensity, according to the work of Haiss and co-workers.[52] These results were further corroborated by analyzing the AuNP size distributions based on transmission electron microscope (TEM) images (13 ± 2 and 35 ± 5 nm, respectively) and dynamic light scattering (DLS) measurements (19 ± 8 and 38 ± 8 nm, respectively), see Fig. 1. The DLS measurements showed bigger mean diameters and wider size distributions for the smaller AuNPs due to the contribution of the solvation shell on the measured hydrodynamic diameter, which is typically higher for smaller NPs, as reported previously.[56,57] Meanwhile, for 38 nm Ø AuNPs all three methods gave comparable and converging results. In addition, the AuNP size distribution broadened and the AuNP concentration dropped drastically (*e.g.*, from 4.0×10^9 particles per μL for 12 nm Ø AuNPs to only 1.1×10^8 particles per μL for 38 nm Ø AuNPs) with the increasing NP size.

Characterization of the interfacial gold nanofilms by extinction and reflection spectra: experimental configurations

In situ UV-Vis-NIR spectra were recorded in two configurations, total transmittance or extinction and total reflectance, using a white integrating sphere, as outlined in Scheme 1. The interfacial gold nanofilms were formed biphasically in the quartz cells, as described in the Experimental section, and fully coated by the droplet of organic solvent on all sides. This was facilitated by a thin layer of water on the walls of the hydrophilic quartz cells allowing the gold nanofilm to spread uniformly over the entire organic droplet surface along the sides and the bottom of the cuvette, see Scheme 1B.

To obtain the *transmission spectrum*, light must pass through two gold nanofilms before entering the integrating sphere (Scheme 1B). The background signal of the organic phase (Scheme 1A) was subtracted from all recorded transmission spectra (Scheme 1B). Subsequently, the obtained values were converted into *extinction spectrum* as follows:

$$\mathrm{Ex} = -\log_{10} T \quad (1)$$

where T is the transmittance of light through two gold nanofilms. Thus, the combination of the 0° angle of incidence and subtraction of the transmission spectra for the organic

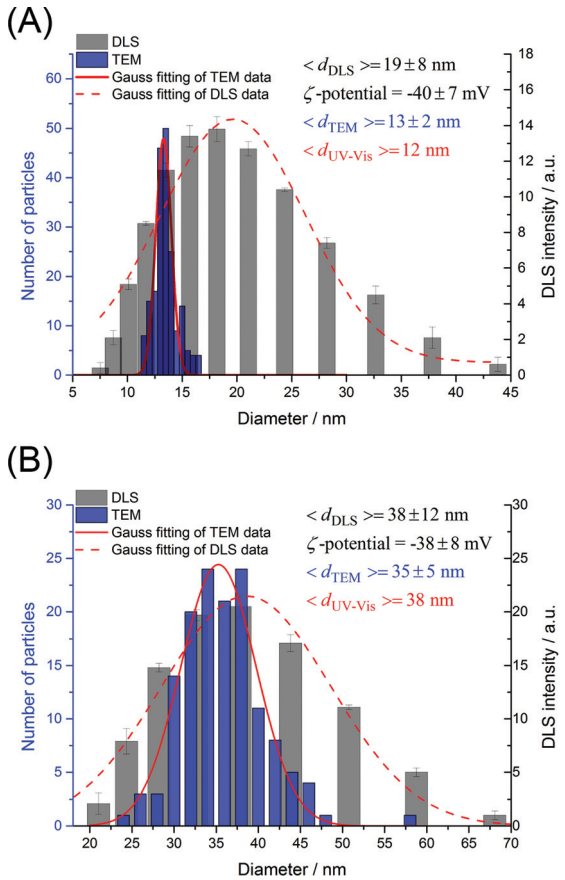

Fig. 1 Characterization of the mean diameters and size distributions of AuNPs synthesized with two mean diameters (A) 12 nm and (B) 38 nm by transmission electron microscopy (TEM) images, dynamic light scattering (DLS) measurements and UV-Vis spectroscopy (as described by Haiss *et al.*).[52]

phase ensured that the influence of light scattering and parasitic reflection at each interface (air-quartz, quartz-water, and water–organic phase), and absorbance of the incident beam in the bulk phase, were minimized. The extinction spectrum of a commercially available blue filter, purchased from ThorLabs (FGB37S), was recorded as depicted in Scheme 1C and used for comparison.

The *reflectance spectrum* was recorded immediately upon completing the acquisition of the extinction spectrum. The extinction spectra were recorded with the incidence beam impinging the surface at an angle 8° to normal. In contrast to the transmission spectra, the reflectance spectra were only due to a single gold nanofilm on one side of the cell (Scheme 1D). The background reflectance spectrum from the organic phase was subtracted to evaluate only the reflectance due to the gold nanofilm (Scheme 1E). The reflectance spectrum of a commercially available gold mirror, purchased from ThorLabs (PF10-03-M01) and separated from the sample-window with a 2 mm quartz plate (the same thickness as the quartz window of the cuvette), was recorded and used as a "reference" corresponding to 100% reflectance (Scheme 1F).

Influence of AuNP mean diameter and interfacial AuNP surface coverage (θ_{int}^{AuNP}) on the extinction and reflectance spectra obtained for interfacial gold nanofilms prepared at water–DCE interfaces

Liquid mirrors based on nanofilms of 38 nm Ø AuNPs. Initially, we comprehensively characterized the extinction (Fig. 2A, C and E) and transmission (Fig. 2B, D and E) spectra obtained for interfacial gold nanofilms formed with the larger 38 nm Ø AuNPs at water–DCE interfaces (in the presence of TTF in the organic solvent droplet) as a function of θ_{int}^{AuNP}. The latter was calculated, as described previously,[24] by (a) assuming that the AuNPs adopt a hexagonal close-packed (HCP) monolayer assembly at the liquid–liquid interface, (b) determining the concentration of the AuNPs present in the aqueous phase (of known volume) by UV-Vis spectroscopy, and (c) approximating the available liquid–liquid surface area as that equivalent to a cube defined by the dimensions of the quartz cuvette, namely, 6 ± 0.2 cm^2.

Briefly, θ_{int}^{AuNP} may be obtained simply as follows:

$$\theta_{int}^{AuNP} = \frac{V_{added}}{V_{HCP}} \quad (2)$$

where V_{added} denotes the added volume of AuNPs of a known concentration, V_{HCP} is the volume of AuNPs of the same concentration required to entirely fill the available interfacial surface with a hexagonal close-packed monolayer. Thus, θ_{int}^{AuNP} is a dimensionless coverage, describing how many monolayers (ML) of AuNPs are adopted by the interface.

The extinction spectra consisted of two bands, indicative of the presence of some separation distances between the AuNPs in the interfacial assembles (discussed in more detail in the transmission electron microscopy (TEM) studies *vide infra*). Firstly, a Localized Surface Plasmon (LSP)-band of individual AuNPs in the interfacial nanofilm was observed with a maximum at *ca.* 560 nm that remained invariant with θ_{int}^{AuNP} (Fig. 2A and C). This band was red-shifted by 35 nm with respect to the LSP-band of the initial aqueous AuNP colloidal solution (the blank dashed curve in Fig. 2A). Secondly, a Surface Plasmon Coupling (SPC)-band was evident with the maximum shifted between *ca.* 770 and *ca.* 850 nm depending on θ_{int}^{AuNP} (Fig. 2A and C). Similarly, the reflectance spectra also possessed two clear bands located at *ca.* 550 and 900 nm which may also be attributed to LSP- and SPC-contributions, respectively (Fig. 2B and D).

Two main processes may affect the extinction LSP-band position: (i) charging of the AuNPs by the redox active TTF molecules that displace the citrate ligands from the surface of the AuNPs and (ii) changing the dielectric permittivity of the surrounding media (again, for example, by substitution of the citrate shell with TTF molecules).[24,58] TTF molecules are efficient electron donors, capable of pumping electrons into the AuNP with concomitant formation of $TTF^{+\bullet}$, followed by Fermi level equilibration.[24,31] Indeed, charging the AuNPs with electrons leads to a blue-shift of the LSP-band. However, as shown by Mulvaney and co-workers,[59,60] a significant blue-

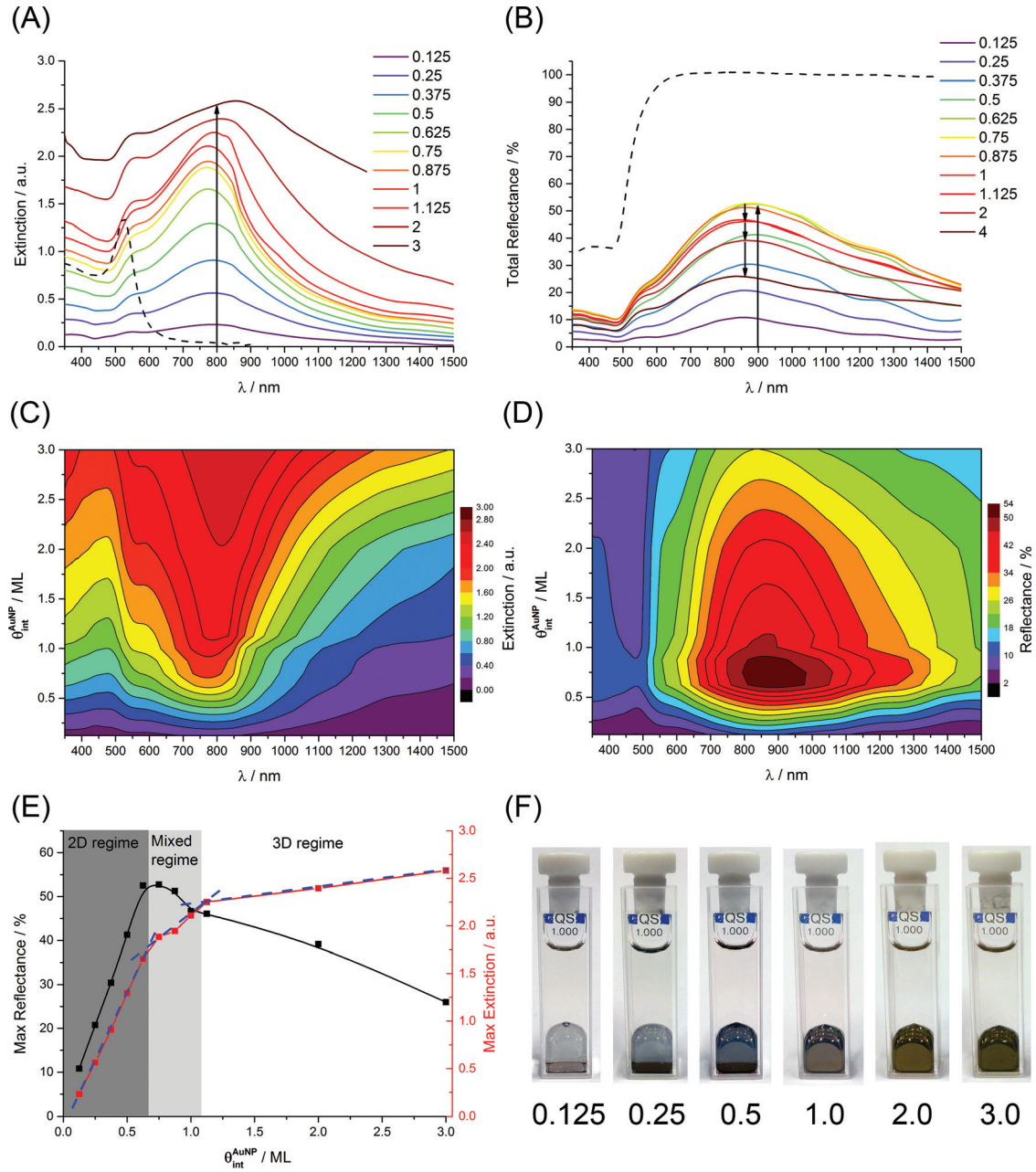

Fig. 2 UV-Vis-NIR optical responses of interfacial gold nanofilms, consisting of 38 nm mean diameter AuNPs, at a water–DCE interface as a function of increasing interfacial AuNP surface coverage θ_{int}^{AuNP}. The DCE phase contains the lipophilic TTF molecule. (A) Extinction spectra: the black dashed line represents the spectra of the aqueous citrate-stabilized colloidal AuNP solution prior to interfacial gold nanofilm formation. (B) Total reflectance spectra: the black dashed line corresponds to reflectance of a solid gold mirror, *i.e.*, acting as a reference representing 100% reflectance. Extinction and reflectance spectra were recorded with the incidence beam impinging the surface at angles of 0° and 8° to normal, respectively. (C, D) Two-dimensional surface contour plots of extinction and reflectance evolution with increasing θ_{int}^{AuNP}. (E) Maximum values of the extinction and reflectance intensities plotted *versus* θ_{int}^{AuNP}. A blue dotted line on the extinction curve denotes linear regions. (F) Photographs demonstrating the clear visible changes in the appearance of the interfacial gold nanofilms with increasing θ_{int}^{AuNP} (values are given in monolayer, ML, as described in the text).

shift requires injection of massive amounts of electrons into the already electron rich AuNPs. A local change of the electrical permittivity or dielectric constant of the surrounding medium may overcome any blue-shift associated with Fermi level equilibration of the AuNPs with TTF molecules and, thus, produce the observed red-shift in the LSP-band on interfacial gold nanofilm formation.[61–65] A shift was observed in the position of the extinction SPC-band maximum from 790 nm for θ_{int}^{AuNP} values corresponding to 1/8 of a monolayer (ML), to 770 nm for 1.0 ML, and subsequently up to 850 nm for

3.0 MLs. Thus, the average position of the SPC-band peak maximum was *ca*. 810 nm. However, it is difficult to establish if this wandering variation of the maximum has a physical origin (*e.g.*, decreasing interparticle distances)[66] or is due to the rearrangements and changes of the local environment of the AuNPs upon nanofilm growth. The plots of the maximum extinction (red data points) and reflectance (black data points) peak intensities *versus* θ_{int}^{AuNP} were highly informative revealing several interesting features in the optical behavior of the interfacial gold nanofilms (Fig. 2E). The steady continuous growths of the overall extinction and reflectance peak intensities with increasing θ_{int}^{AuNP} were both abruptly interrupted under 0.625 ML conditions. At this initial threshold the linear dependence (the Beer–Lambert law) was broken for the extinction spectra causing a change of slope or, in other words, the extinction coefficient (Fig. 2E, red data points). A second threshold was reached under 1.125 ML conditions, again leading to a further change of the slope. Thus, three distinct regions were distinguished, each with a unique extinction coefficient; (1) a 2D regime dominated by smooth "floating islands" of interfacially adsorbed 2D monolayers, (2) a mixed 2D/3D regime where the 2D "floating islands" start to become modified with 3D nanostructures consisting of small piles of adsorbed AuNPs even under sub-full-monolayer conditions, and (3) a 3D regime where the interfacially adsorbed 2D full-monolayer is completely subsumed beneath significant piles of adsorbed AuNPs. The presence of these three distinct regimes is further supported by *ex situ* scanning electron microscopy (SEM) images of the interfacial gold nanofilms after their transfer to silicon substrates, discussed *vide infra*.

The variation of the reflectance in these three regimes is marked (Fig. 2E, black data points). As noted, the reflectance increases steadily with increasing θ_{int}^{AuNP} in the 2D regime. In the mixed 2D/3D regime the rate of increase in reflectance slows dramatically and reaches a maximum of 51% (compared to the 100% reference reflectance from the Thorlabs gold mirror) between 0.75 and 0.875 ML conditions, followed by a slow decrease under 1.125 ML conditions. Beyond this, in the 3D regime, the rate of decrease of reflectance ramps up significantly, and this behavior is clearly visible to the naked eye with a dimming of the luster of the interfacial gold nanofilms between 1.0 and 3.0 ML conditions (Fig. 2F).

From the spectroscopic point of view, the overall peak width of the extinction and reflectance spectra broaden with increasing θ_{int}^{AuNP} beyond 1.0 ML conditions. This is indicative of the formation of additional out-of-plane interactions between AuNPs. Owing to the the morphology of the interfacial gold nanofilm transitions from 2D to 3D beyond 1.0 ML conditions, each AuNP (surrounded by six close neighbors in the interfacially adsorbed 2D monolayer) establishes contact with three further AuNPs in the second layer leading to additional depolarization factors and peak broadening. The latter is supported by previous simulations and experimental observations demonstrating that increasing the extent of interacting AuNPs leads to a red shift and broadening of the SPC-peak.[3,12,13,67] Under these conditions both red and green lights were absorbed strongly (Fig. 2A and C) which also leads to strong reflection of these two colours (Fig. 2B and D). The human eye then perceives these mixtures of red and green lights as orange or gold, giving the strong golden coloration of the multilayer nanofilms, see Fig. 2F.

Liquid filters based on nanofilms of 12 nm Ø AuNPs. Subsequently, we comprehensively characterized the extinction (Fig. 3A, C and E) and transmission (Fig. 3B, D and E) spectra obtained for interfacial gold nanofilms formed with the smaller 12 nm Ø AuNPs at water–DCE interfaces (in the presence of TTF in the organic solvent droplet) as a function of θ_{int}^{AuNP}. All of the trends found for the larger AuNPs were generally replicated. In addition, the extinction spectra exhibited both LSP- and SPC-bands at *ca.* 550 nm and *ca.* 690 nm, respectively. The LSP-band was slightly (10 nm) blue-shifted, while the SPC-band was significantly (120 nm) blue-shifted in comparison with the interfacial gold nanofilms formed with 38 nm Ø AuNPs. The LSP-band appeared as a tiny shoulder on the intense and broad SPC-band and was only visible under high θ_{int}^{AuNP} conditions in excess of 1 ML (Fig. 3A). Also, variation in the position of the SPC-band maximum was observed to be quite small under sub-ML conditions: *ca.* 680 nm for θ_{int}^{AuNP} of 0.16 ML to *ca.* 675 nm for θ_{int}^{AuNP} of 0.33 ML. However, the maximum of the SPC-band reached *ca.* 720 nm for 4 MLs.

The reflectance spectra also possessed two bands attributed to LSP- and SPC-contributions, respectively (Fig. 3B and D). The trends seen for the variations of the extinction and reflectance peak intensities *versus* θ_{int}^{AuNP} were replicated with the three distinct regimes, discussed above, again evident (Fig. 3E). In this instance the maximum values of both the extinction and reflectance spectra simultaneously changed the slope under *ca.* 0.83 ML conditions.

Although, the observed trends in the optical behavior for interfacial gold nanofilms formed with either 12 or 38 nm Ø AuNPs were broadly similar, some clear distinctions exist that impact their potential applications. Interfacial nanofilms formed with 38 nm Ø AuNPs display (a) considerably broader SCP extinction bands under θ_{int}^{AuNP} conditions in excess of 1 ML (leading to their gold coloration) and (b) a maximum reflectance of 51% *versus* only 24% for 12 nm Ø AuNPs. Hence, 12 nm Ø and smaller AuNPs are good candidates to form optical filters at liquid–liquid interfaces, whereas 38 nm Ø and larger AuNPs may potentially be utilized to form optical mirrors at liquid–liquid interfaces.

Monitoring the morphology of the interfacial gold nanofilms with increasing θ_{int}^{AuNP} by scanning electron microscopy (SEM)

The interpretation of the extinction and reflectance spectra for interfacial nanofilms formed with 38 nm Ø (Fig. 2) and 12 nm Ø (Fig. 3) AuNPs was dependent on the existence of 3 distinct morphological regimes of the AuNPs at the interface, each of which scattered light to varying degrees, as a function of θ_{int}^{AuNP}.

To confirm their existence we transferred interfacial gold nanofilms formed in a stepwise manner with 38 nm Ø AuNPs under a series of θ_{int}^{AuNP} conditions (from 0.1 to 2.0 ML) to silicon substrates, as described in the Experimental section,

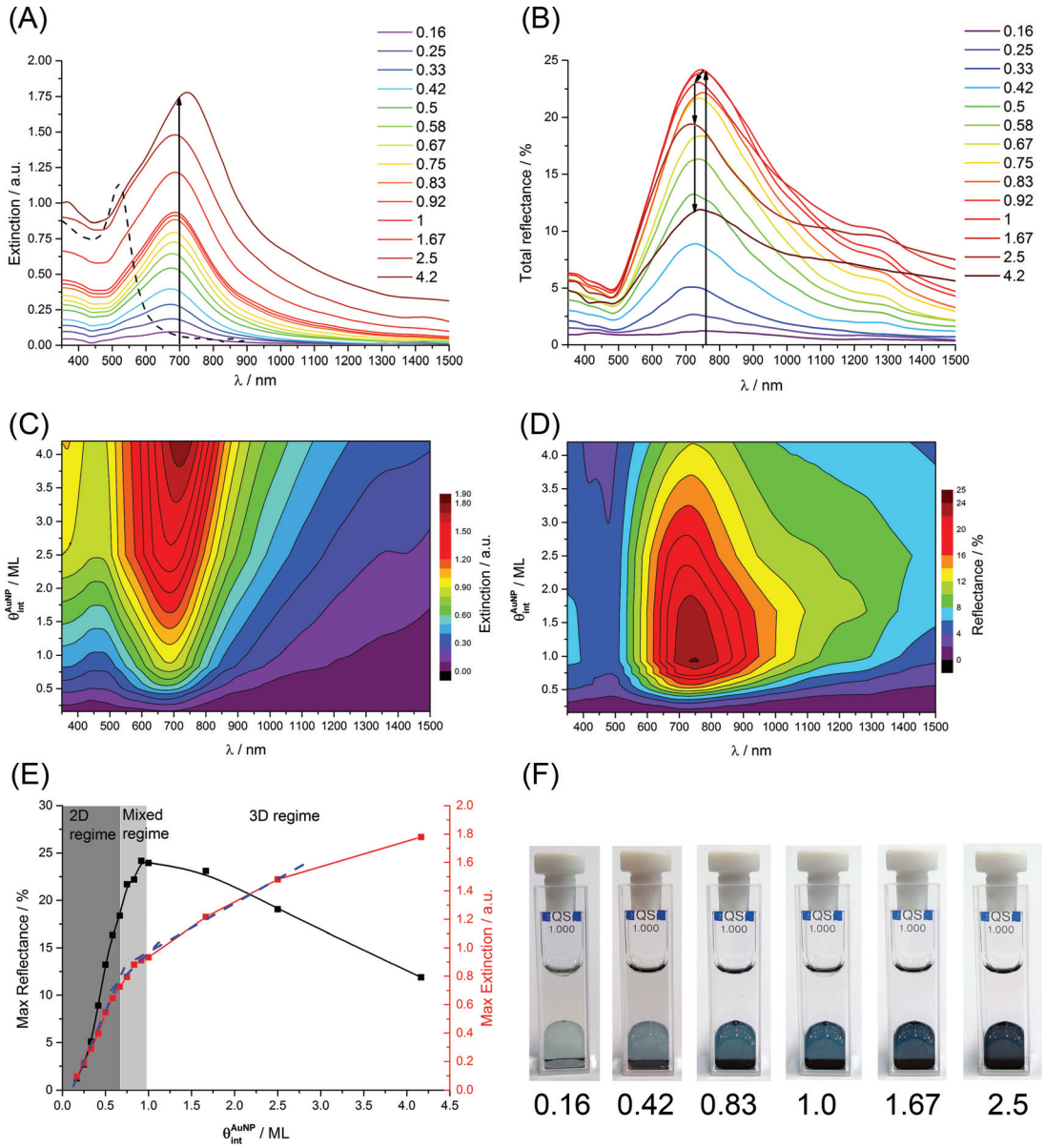

Fig. 3 UV-Vis-NIR optical responses of interfacial gold nanofilms, consisting of 12 nm mean diameter AuNPs, at a water–DCE interface as a function of increasing interfacial AuNP surface coverage (θ_{int}^{AuNP}). The DCE phase contains the lipophilic TTF molecule. (A) Extinction spectra: the black dashed line represents the spectra of the aqueous citrate-stabilized colloidal AuNP solution prior to interfacial gold nanofilm formation. (B) Total reflectance spectra: the reflectance is normalized with respect to the reflectance of a solid gold mirror, *i.e.*, acting as a reference representing 100% reflectance. Extinction and reflectance spectra were recorded with the incidence beam impinging the surface at angles of 0° and 8° to normal, respectively. (C, D) Two-dimensional surface contour plots of extinction and reflectance evolution with increasing θ_{int}^{AuNP}. (E) Maximum values of the extinction and reflectance intensities plotted *versus* θ_{int}^{AuNP}. A blue dotted line on the extinction curve denotes linear regions. (F) Photographs demonstrating the clear visible changes in the appearance of the interfacial gold nanofilms with increasing θ_{int}^{AuNP} (values are given in monolayer, ML, as described in the text).

and obtained the SEM images of each (Fig. 4A). Also *in situ* optical microscopy observations were carried out to confirm the SEM results (selected images are presented in Fig. 4 and a full detailed description is given in Fig. S1, section 1 of the ESI†).

At low θ_{int}^{AuNP}, the AuNPs were organized in low density monolayers of both interconnected and isolated 2D "floating islands" (0.1 ML, Fig. 4A). As θ_{int}^{AuNP} increased to 0.4 ML the AuNPs filled the majority of available space with some empty voids still being observed (0.4 ML, Fig. 4A). Previously, we predicted that beyond the θ_{int}^{AuNP} values of 0.5 ML, the floating networks of AuNPs at the interface establish electrically connected pathways, transitioning from insulating to locally electrically conductive structures.[68] Up to 0.6 ML conditions the interfacial gold nanofilm was predominantly 2D in nature (section 1 in the ESI†), with very few 3D AuNP structures

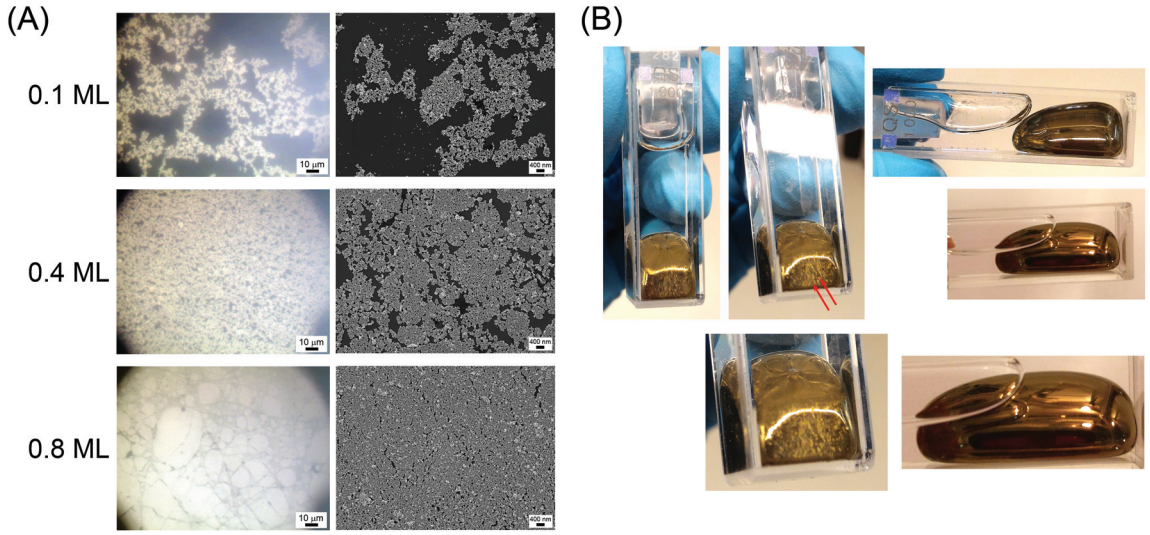

Fig. 4 Macro- and nano-scale mechanisms of decreasing reflectance caused by morphological changes. (A) Comparison of optical microscopy images (50× magnification) performed *in situ* at the AuNP nanofilm modified liquid–liquid interface and SEM images of these nanofilms transferred to a silicon substrate for selected θ_{int}^{AuNP}. 3D piles of AuNPs were seen as brighter dots. Scale bars are, from left to right, 10 μm and 400 nm, respectively. (B) Photographs highlighting the wrinkles (red arrows) that appear in the interfacial gold nanofilm (1 ML) surrounding the organic droplet as a consequence of mechanical forces acting on the nanofilm within the confined environment of the quartz cuvette (on the left). Wrinkles disappear upon surface extension (on the right).

present (and none of substantial size) to induce scattering. Hence, the reflectance increased smoothly as observed in Fig. 2E to this point and was denoted as the 2D regime.

At 0.8 ML, in the mixed 2D/3D regime, the interfacial AuNP film was very dense, with few voids present, and a small but notable quantity of AuNPs now forming 3D piles on the surface of the underlying 2D AuNP monolayer (0.8 ML, Fig. 4A). As seen in the optical image, densely-packed areas co-existed with less dense "diffuse" areas. Despite the fact that the interfacial gold nanofilm at 0.8 ML is theoretically 20% below the value expected for complete coverage of the liquid–liquid interface with AuNPs in a hexagonal close-packing arrangement, this θ_{int}^{AuNP} for 38 nm Ø AuNPs exhibited the maximum values for reflectance, see Fig. 2E.

Under these conditions maximum coverage of the interface with the 2D monolayer (enhancing reflectance) was attained without the presence of notable quantities of 3D piles of AuNPs that cause the incident light to scatter (diminishing reflectance).

Finally, moving into the 3D regime at θ_{int}^{AuNP} of 1.0 and 2.0 ML (section 1 in the ESI†), the additional AuNPs now presented at the interface could no longer directly adsorb there as it is effectively saturated with AuNPs. Thus, the 3D piles of AuNPs grew on the underlying 2D monolayer, rapidly proliferated and increased substantially in terms of their footprint and height. The resultant increase in scattering significantly diminished the reflective luster of the gold nanofilms, causing them to visually become less reflective to the naked eye (Fig. 2F).

A second factor that may decrease the reflectance at θ_{int}^{AuNP} higher than 0.8 ML is the presence of wrinkles in the interfacial gold nanofilms due to the mechanical stresses placed on the nanofilms within the confined environment of the quartz cuvette. As demonstrated in Fig. 4B, these wrinkles are visible to the naked eye after the biphasic preparation procedure, detailed in the Experimental section. Such buckling of the interfacial gold nanofilm by mechanical stress is similar to that observed for compressed NP films in Langmuir–Blodgett baths.[69–71] Wrinkles arise as the close-packed interfacial AuNP 2D-layer is a quasi-stable system and can respond to compression forces by buckling. Additionally, to respond to external disturbances, the packing arrangement of the interfacially adsorbed AuNPs may be adjusted. For example, AuNP assemblies with cubic close packing or random close packing are relatively flexible, and, as a consequence, may suppress to some extent the external mechanical forces through temporary and local transformation to hexagonal close packed arrangements (a rigid system without any free space available for AuNPs to move or relocate, except buckling).

Determining the separation distances between AuNPs in the interfacial gold nanofilms by high resolution transmission electron microscopy (HR-TEM)

The presence of two clear bands in the extinction and reflectance spectra for interfacial gold nanofilms formed with 38 nm Ø AuNPs (Fig. 2A and B) is evidence to show that a separation distance exists between these AuNPs within interfacial assemblies. Also, although not as clearly evident for 12 nm Ø AuNPs (Fig. 3A and B), two bands were also shown to exist in the spectra. Several research groups have shown both experimentally and theoretically, through modeling of optical responses for metallic NP assemblies, that extremely low or

zero interparticle distances result in a broad band in the reflectance spectra tailing into the NIR range, as seen for bulk mirrors.[3,13,72] In contrast, relatively large interparticle distances lead to a bell-shaped reflectance in the middle of the UV-Vis spectra. Thus, tuning of interparticle distances is a direct way of controlling the optical response of metallic NP assemblies.[3,13,72]

The interparticle separation distance distributions were measured by HR-TEM and are presented in Fig. 5. For interfacial gold nanofilms formed with either 12 or 38 nm Ø AuNPs, the interparticle separation distances were estimated to be 0.85 (±0.1) and 0.87 (±0.2) nm, respectively. These distances were equivalent to the thickness of a few layers of π-stacked TTF or $TTF^{+\bullet}$ molecules that form a shell around each AuNP. Thus, while the AuNPs are located in close enough proximity with each other in the interfacial nanofilm to lead to effective electronic coupling between the individual AuNPs, they do not touch each other.[3,13,72] This is a key attribute of these nanofilms making them an attractive soft interfacial substrate for mirror applications and future SERS studies in particular.[73,74]

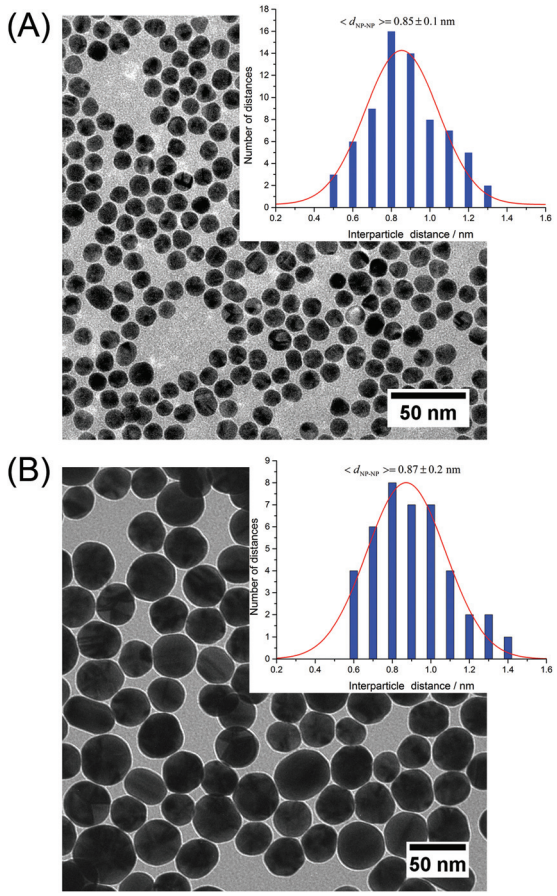

Fig. 5 High-resolution transmission electron microscopy (HR-TEM) images of interfacial gold nanofilms after transferring to a TEM grid. The interfacial gold nanofilms were formed with (A) 12 and (B) 38 nm Ø AuNPs at the water–DCE interface, with TTF present in the organic droplet, and at 0.8 ML conditions. Insets: interparticle separation distance distributions were measured based on the HR-TEM-images.

Comparing the optical responses of interfacial gold nanofilms formed biphasically using alternative organic solvents of low miscibility with water and replacing the lipophilic molecule TTF in the organic droplet with neocuproine (NCP)

Thus far we have focused entirely on thoroughly characterizing our initial organic solvent/lipophilic molecule combination of DCE containing TTF.[24] In this final section, we demonstrate that our biphasic approach to interfacial gold nanofilm formation, whereby the citrate ligands are displaced from the surface of the aqueous AuNPs by a lipophilic species present in the organic solvent, is not restricted to the combination noted above.

Initially, we expanded our choice of organic solvents under investigation to include α,α,α-trifluorotoluene (TFT), nitrobenzene (NB), and nitromethane ($MeNO_2$). These solvents differ in the density (ρ), dielectric constant in a static electric field (ε_r) and interfacial surface tension ($\gamma_{w/o}$) to 1,2-dichloroethane (DCE). Thus, the goal here was to determine the magnitude of the influence of the immiscible organic solvent on the observed optical responses and the stability of the interfacial gold nanofilms $\gamma_{w/o}$ was measured for each water–organic solvent interface by the pendant drop method (Fig. S2, section 2 in the ESI†). With the exception of $MeNO_2$, each of these liquid–liquid interfaces are polarizable (either chemically or electrochemically) and, thus, may be implemented in the construction of electrically driven "smart" filters and mirrors.[39] Relevant physiochemical data on each organic solvent and water–organic solvent interface are summarized in Table 1.

Subsequently, the lipophilic molecule neocuproine (NCP), previously used to self-assemble AgNPs at water–DCE interfaces,[6,7] was tested and the interfacial gold nanofilms formed were compared to those observed at water–DCE interfaces with TTF in the organic phase. We also investigated other bipyridines, previously reported to create liquid mirror films of AgNPs,[6,76,77] and thionine,[78] a direct structural analogue of TTF. However, only NCP led to interfacial AuNP nanofilm formation and is thus the sole focus of our extended analysis herein.

Comparison of the extinction and reflectance spectra for interfacial gold nanofilms formed with either 12 nm Ø (Fig. 6A and B) or 38 nm Ø (Fig. 6B and D) AuNPs, using either DCE,

Table 1 Summary of the density (ρ) and dielectric constant in a static electric field (ε_r)[75] of each organic solvent studied, and the interfacial surface tension ($\gamma_{w/o}$) of each water–organic solvent interface (as determined by the pendant drop method in section 2 of the ESI)

Solvent	ρ/g cm^{-3}	ε_r[75]	$\gamma_{w/o}$/mN m^{-1}
TFT	1.181	9.18	38.0 ± 0.5
DCE	1.256	10.42	30.5 ± 0.3
NB	1.552	35.60	24.4 ± 0.2
$MeNO_2$	1.130	37.27	16.0 ± 0.2

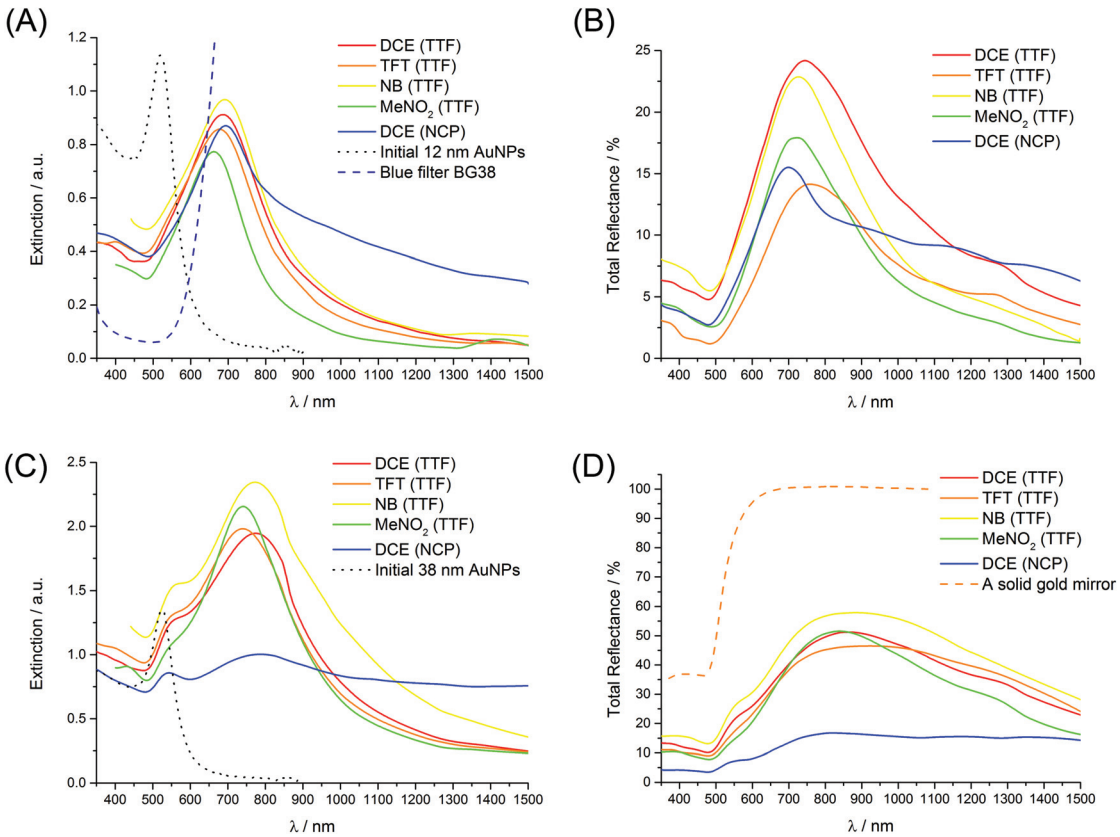

Fig. 6 Monitoring the influence of the immiscible organic solvent and lipophilic molecule in the organic droplet on the optical responses of the interfacial gold nanofilms. (A) Extinction and (B) reflectance spectra for interfacial gold nanofilms formed with 12 nm Ø AuNPs. (C) Extinction and (D) reflectance spectra for interfacial gold nanofilms formed with 38 nm Ø AuNPs. The organic solvents investigated were DCE, TFT, NB and $MeNO_2$. The lipophilic molecules TTF or NCP were present in each organic droplet and optimal values of θ_{int}^{AuNP}, in terms of maximum reflectance for interfacial gold nanofilms formed at water–DCE interfaces (determined in Fig. 2 and 3) of 0.75 ML were implemented. For comparison, the extinction spectra of a solid blue filter, dashed blue line in (A), and reflectance spectra of a solid gold mirror, dashed gold line in (D), are shown.

TFT, NB or $MeNO_2$ as the organic solvent, are presented in Fig. 6.

Optical photographs of the obtained interfacial gold nanofilms are given in Fig. S3, section 3 of the ESI.† A value of 0.75 for θ_{int}^{AuNP}, at the beginning of the mixed 2D/3D regime with interfacial gold nanofilms formed at water–DCE interfaces, was chosen in all instances to achieve maximum reflectance, discussed *vide supra*. The maximum extinction intensity and percentage reflectance for each interfacial AuNP film under 0.75 ML conditions are summarized in Table 2.

As demonstrated in Fig. 6 and Table 2, the various solvents influenced the interfacial AuNP film formation to some extent, but under 0.75 ML conditions, the extinction and reflectance spectra were broadly similar with no major changes in the shapes of either spectra and relatively narrow distributions observed for the maximum extinction (between 0.77 and 0.91 a.u. for 12 nm Ø AuNPs, and 1.95 and 2.16 a.u. for 38 nm Ø AuNPs) and maximum reflectance (between 14.2 and 22.9% for 12 nm Ø AuNPs, and 46.5 and 58% for 38 nm Ø AuNPs). Thus, in terms of developing self-healing optical mirrors, water–NB interfaces with 38 nm Ø AuNPs marginally gave the best reflectance values (58%). Also, in terms of optical filter applications, again water–NB interfaces with 12 nm Ø AuNPs exhibited the highest extinction intensities at *ca.* 690 nm.

A notable observation, highlighted in Fig. S3, section 3 in the ESI,† was the self-assembly of interfacial AuNP films at water–$MeNO_2$ interfaces even in the absence of the lipophilic TTF molecule in the organic droplet. A similar observation was recently reported for AuNPs at water–1-butanol interfaces.[79] One possibility is that $MeNO_2$ molecules competitively adsorb onto the surface of the AuNPs,[80–82] in a similar manner to TTF displacing the citrate ligands, reducing the surface charge of the AuNPs enough to facilitate their adsorption at the interface driven by minimization of the total interfacial free energy.[83]

A second observation was that at the θ_{int}^{AuNP} values in excess of 1 ML, for both 12 and 38 nm Ø AuNPs, the interfacial AuNP films formed at water–TFT interfaces completely lost their metallic luster and turned black due to massively increased scattering of the incident light, see Fig. S4, section 4 in the ESI.† The interface itself appeared rough either due to the presence of large AuNP agglomerates due to the uncontrolled aggregation of the AuNPs in the interfacial film, or perhaps due to

Table 2 Comparison of the maximum extinction (a.u.) and reflectance (%) values measured for interfacial gold nanofilms, consisting of either 12 nm or 38 mean diameter AuNPs, formed with either DCE, TFT, NB or $MeNO_2$ as the organic solvent. The lipophilic molecules TTF or NCP were present in each organic droplet and θ_{int}^{AuNP} values of 0.75 ML were implemented. The peak positions at which each of the values were determined from the spectra shown in Fig. 6 are indicated in brackets

		12 nm Ø AuNPs		38 nm Ø AuNPs	
Solvent	Lipophilic molecule	Extinction/a.u.	Reflectance/%	Extinction/a.u.	Reflectance/%
DCE	NCP	0.87 (693 nm)	15.5 (699 nm)	1.00 (787 nm)	16.8 (822 nm)
DCE	TTF	0.91 (685 nm)	24.2 (745 nm)	1.95 (774 nm)	51.2 (864 nm)
TFT	TTF	0.86 (677 nm)	14.2 (757 nm)	1.98 (740 nm)	46.5 (906 nm)
NB	TTF	0.97 (691 nm)	22.9 (728 nm)	2.34 (773 nm)	58 (884 nm)
$MeNO_2$	TTF	0.77 (662 nm)	17.9 (723 nm)	2.16 (741 nm)	51.6 (838 nm)

buckling of the water–TFT interface at these high θ_{int}^{AuNP} values. The origin of this behavior is, as yet, unresolved. As detailed in Table 1, however, TFT has the highest interfacial surface tension among the considered solvents of 38 mN m^{-1} and the impact of increased interfacial surface tension to potentially induce buckling of the interfacial gold nanofilms at high interfacial surface coverages is discussed in section 4 of the ESI.†

A comparison of the extinction and reflectance spectra for interfacial gold nanofilms formed biphasically with either 12 or 38 nm Ø AuNPs and with either NCP (blue spectra) (see Fig. S5, section 5 in the ESI† for the chemical structure of NCP) or TTF (red spectra) in the DCE droplet are also presented in Fig. 6 and Table 2. Again, θ_{int}^{AuNP} values of 0.75 ML were chosen. The extinction spectra for interfacial nanofilms composed of 12 nm Ø AuNPs revealed a significant tailing into the NIR region when NCP was present in the DCE droplet (Fig. 6A).

Additionally, the reflectance of these nanofilms with NCP present was less than that observed with TTF, dropping from 24.2 to 15.5% (Fig. 6B). For 38 nm Ø AuNPs, major optical differences were observed for the interfacial gold nanofilms, with the appearance of a strong broadband absorption (Fig. 6) and a huge drop in reflectance, from 51.2% to 16.8% (Fig. 6D), when NCP was replaced with TTF in the DCE droplet. These observations indicate that the AuNPs in the interfacial gold nanofilm formed with NCP were in extremely close proximity, with considerably smaller interparticle separation distances than those with TTF in the DCE droplet. These small interparticle distances led to strong interparticle plasmonic coupling, which in turn cause broadband absorption, low reflectivity and the interfacial gold nanofilms to appear very dark in color, resembling "black gold" (see Fig. S5, section 5 in the ESI† for optical photographs of the obtained interfacial gold nanofilms), as recently described by Liu *et al.*[79] Clearly, these "black gold" films are not suitable for either optical mirror or filter applications. However, their lower reflectance and, in particular, strong ability to absorb light in the NIR range leading to their enhanced broadband absorption, means that they may potentially impact other technological niches, such as photothermal therapy,[84,85] bio-imaging, and targeted drug delivery.[86,87]

Conclusions

The influence of a host of experimental variables (AuNP mean diameter, Ø; interfacial AuNP surface coverage θ_{int}^{AuNP}; the nature of the organic solvent; nature of the lipophilic organic molecule that caps the AuNPs in the interfacial nanofilm) on the optical properties of interfacial gold nanofilms formed at immiscible water–oil interfaces were investigated by both *in situ* spectroscopy (extinction and reflection UV-vis-NIR spectra and optical photographs) and *ex situ* microscopy (TEM and SEM images of interfacial gold nanofilms transferred to silicon substrates) techniques.

Smaller AuNPs with 12 nm Ø were suited to applications as liquid based optical band-pass filters, forming interfacial gold nanofilms that attenuated green and red lights, while transmitting blue light. Larger AuNPs with 38 nm Ø were suited to applications as liquid mirrors, forming interfacial gold nanofilms that strongly reflected both red and green light, perceived as gold to the human eye.

The magnitudes of the maximum reflection for interfacial gold nanofilms formed, determined by *in situ* UV-vis-NIR spectra, were strongly influenced by the morphology of the nanofilms at the interface, which was in turn determined by θ_{int}^{AuNP}. Systematic *in situ* spectroscopy studies, corroborated by *in situ* optical micrographs and *ex situ* SEM images, revealed three distinct morphological regimes, with optimal conditions being those that yielded the maximum coverage of the interface with a 2D monolayer (enhancing reflectance) without the presence of notable quantities of 3D piles of AuNPs that cause the incident light to scatter (diminishing reflectance). For water–DCE interfaces this was determined to be at a submonolayer (ML) surface coverage (approximately 0.75 ML) assuming hexagonal close packing of the AuNPs at the interface.

The nature of the organic solvent turned out to be the least influential variable studies, with only small variations of maximum extinction and reflectance observed in both 12 and 38 nm Ø AuNPs at 0.75 ML surface coverages when DCE was replaced with TFT, $MeNO_2$ or NB. Interesting aberrations included the observation of interfacial gold nanofilms with $MeNO_2$ without a lipophilic molecule in the organic droplet (typically required to displace the citrate ligands and induce

biphasic nanofilm formation with all other organic solvents). This was attributed to $MeNO_2$ molecules competitively adsorbing onto the AuNPs surface, displacing citrate ligands. Also, water–TFT interfaces completely lost their metallic luster, turning black in colour, due to massively increased scattering of the incident light at high θ_{int}^{AuNP}. A possible reason for this behavior may be linked to the water–TFT interfaces having the highest surface tension of any of the organic solvents investigated and, thus, the interfacial gold nanofilm formed may be more prone to buckling and wrinkling. Finally, for optical mirrors, water–NB interfaces with 38 nm Ø AuNPs marginally gave the best reflectance values (58%) and, for optical filters, again water–NB interfaces with 12 nm Ø AuNPs exhibited the highest extinction intensities at *ca.* 690 nm.

The interparticle spacing within the interfacial gold nanofilm was varied by replacing the lipophilic molecule TTF with NCP) in the organic droplet. This caused major drops in the reflectance of the interfacial gold nanofilms (especially with the 38 nm Ø AuNPs), tailing into the NIR region with the 12 nm Ø AuNPs, and a strong broadband absorbance with the 38 nm Ø AuNPs. All these observations indicated that the interparticle spacing decreased to such an extent with NCP as the capping ligand that the resulting strong interparticle plasmon coupling led to the formation of "black gold" nanofilms with the larger AuNPs.

All-in-all, we showed that by judicious choice of the experimental variables outlined above, the reflectance and extinction of interfacial gold nanofilms could be varied and optimized, creating self-healing nanofilms with potential applications ranging from optical filters and mirrors, SERS substrates for sensors, enhancing non-linear SHG responses, photothermal therapy, bio-imaging, and targeted drug delivery, as discussed *vide infra*.

Acknowledgements

We would like to acknowledge financial support from the Fondazione Oronzio e Niccolò De Nora, Swiss National Science Foundation (Solar Fuel 2000-20_152 557/1). This publication has emanated from research by M. D. S. supported in part by a research grant from the Science Foundation Ireland (SFI) under the Grant Number 13/SIRG/2137. Dr Elham Ghadiri (EPFL) and Prof. Jacques-Edouard Moser (EPFL) are thanked for their help in carrying out the UV-Vis-NIR experiments. Dr Christophe Roussel (EPFL) is thanked for fruitful discussion on technical principles of UV-Vis-NIR spectroscopy and Dr Colm O'Dwyer (Chemistry Department and Tyndall National Institute, University College Cork) is acknowledged for productive discussions on the physics of light interaction processes.

Notes and references

1 H. A. Macleod, *Thin-Film Optical Filters*, CRC Press, 4th edn, 2010.
2 Z. A. Khan, R. Kumar, W. S. Mohammed, G. L. Hornyak and J. Dutta, *J. Mater. Sci.*, 2011, **46**, 6877–6882.
3 T. Ung, L. M. Liz-Marzán and P. Mulvaney, *J. Phys. Chem. B*, 2001, **105**, 3441–3452.
4 E. F. Borra, O. Seddiki, R. Angel, D. Eisenstein, P. Hickson, K. R. Seddon and S. P. Worden, *Nature*, 2007, **447**, 979–981.
5 P.-P. Fang, S. Chen, H. Deng, M. D. Scanlon, F. Gumy, H. J. Lee, D. Momotenko, V. Amstutz, F. Cortés-Salazar, C. M. Pereira, Z. Yang and H. H. Girault, *ACS Nano*, 2013, **7**, 9241–9248.
6 J. Gingras, J.-P. Déry, H. Yockell-Lelièvre, E. F. Borra and A. M. Ritcey, *Colloids Surf., A*, 2006, **279**, 79–86.
7 Y. Yen, T. Lu, Y. Lee, C. Yu, Y. Tsai, Y. Tseng and H. Chen, *ACS Appl. Mater. Interfaces*, 2014, **6**, 4292–4300.
8 R. A. Taylor, T. P. Otanicar, Y. Herukerrupu, F. Bremond, G. Rosengarten, E. R. Hawkes, X. Jiang and S. Coulombe, *Appl. Opt.*, 2013, **52**, 1413–1422.
9 X. Zhang, C. A. Marocico, M. Lunz, V. A. Gerard, Y. K. Gun'ko, V. Lesnyak, N. Gaponik, A. S. Susha, A. L. Rogach and A. L. Bradley, *ACS Nano*, 2014, **8**, 1273–1283.
10 S. K. Ghosh and T. Pal, *Chem. Rev.*, 2007, **107**, 4797–4862.
11 I. Cohanoschi, A. Thibert, C. Toro, S. Zou and F. E. Hernández, *Plasmonics*, 2007, **2**, 89–94.
12 S. P. Scheeler, S. Mühlig, C. Rockstuhl, S. Bin Hasan, S. Ullrich, F. Neubrech, S. Kudera and C. Pacholski, *J. Phys. Chem. C*, 2013, **117**, 18634–18641.
13 T. Ung, L. M. Liz-Marzán and P. Mulvaney, *Colloids Surf., A*, 2002, **202**, 119–126.
14 H. Duan, D. Wang, D. G. Kurth and H. Mohwald, *Angew. Chem., Int. Ed.*, 2004, **116**, 5757–5760.
15 L. Cheng, A. Liu, S. Peng and H. Duan, *ACS Nano*, 2010, **4**, 6098–6104.
16 W. H. Binder, *Angew. Chem., Int. Ed.*, 2005, **44**, 5172–5175.
17 J. B. Edel, A. A. Kornyshev and M. Urbakh, *ACS Nano*, 2013, **7**, 9526–9532.
18 A. Böker, J. He, T. Emrick and T. P. Russell, *Soft Matter*, 2007, **3**, 1231.
19 D. Wang, H. Duan and H. Möhwald, *Soft Matter*, 2005, **1**, 412–416.
20 G. Amarandei, I. Clancy, C. O'Dwyer, A. Arshak and D. Corcoran, *ACS Appl. Mater. Interfaces*, 2014, **6**, 20758–20767.
21 A. A. J. Olaya, D. Schaming, P.-F. Brevet, H. Nagatani, T. Zimmermann, J. Vanicek, H.-J. Xu, C. P. Gros, J.-M. Barbe and H. H. Girault, *J. Am. Chem. Soc.*, 2012, **134**, 498–506.
22 P. Peljo, L. Murtomäki, T. Kallio, H.-J. Xu, M. Meyer, C. P. Gros, J.-M. Barbe, H. H. Girault, K. Laasonen and K. Kontturi, *J. Am. Chem. Soc.*, 2012, **134**, 5974–5984.
23 F. Reincke, S. G. Hickey, W. K. Kegel and D. Vanmaekelbergh, *Angew. Chem., Int. Ed.*, 2004, **43**, 458–462.
24 E. Smirnov, M. D. Scanlon, D. Momotenko, H. Vrubel, M. A. Méndez, P.-F. Brevet and H. H. Girault, *ACS Nano*, 2014, **8**, 9471–9481.

25 E. Bormashenko, *Curr. Opin. Colloid Interface Sci.*, 2011, **16**, 266–271.
26 J. B. Edel, A. A. Kornyshev, R. Kucernak and M. Urbakh, *Chem. Soc. Rev.*, 2016, **45**, 1581–1596.
27 M. Gadogbe, S. M. Ansar, I.-W. Chu, S. Zou and D. Zhang, *Langmuir*, 2014, **30**, 11520–11527.
28 D. Yogev and S. Efrima, *J. Phys. Chem.*, 1988, **92**, 5754–5760.
29 Y.-K. Park and S. Park, *Chem. Mater.*, 2008, **20**, 2388–2393.
30 Y.-K. Park, S.-H. Yoo and S. Park, *Langmuir*, 2007, **23**, 10505–10510.
31 E. Smirnov, P. Peljo, M. D. Scanlon and H. H. Girault, *ACS Nano*, 2015, **9**, 6565–6575.
32 V. A. Turek, M. P. Cecchini, J. Paget, A. R. Kucernak, A. A. Kornyshev and J. B. Edel, *ACS Nano*, 2012, **6**, 7789–7799.
33 T. P. Bigioni, X.-M. Lin, T. T. Nguyen, E. I. Corwin, T. A. Witten and H. M. Jaeger, *Nat. Mater.*, 2006, **5**, 265–270.
34 B. Kowalczyk, I. Lagzi and B. A. Grzybowski, *Nanoscale*, 2010, **2**, 2366–2369.
35 M. Olson, A. Coskun, R. Klajn, L. Fang, S. K. Dey, K. P. Browne, B. Grzybowski and J. F. Stoddart, *Nano Lett.*, 2009, **9**, 3185–3190.
36 V. Sashuk, R. Hołyst, T. Wojciechowski, E. Górecka and M. Fiałkowski, *Chemistry*, 2012, **18**, 2235–2238.
37 Y. Liu, X.-M. Lin, Y. Sun and T. Rajh, *J. Am. Chem. Soc.*, 2013, **135**, 3764–3767.
38 C. Zhou and Y. Li, *J. Colloid Interface Sci.*, 2013, **397**, 45–64.
39 M. E. Flatte, A. A. Kornyshev and M. Urbakh, *J. Phys. Chem. C*, 2010, **114**, 1735–1747.
40 J.-P. Abid, M. Abid, C. Bauer, H. H. Girault and P.-F. Brevet, *J. Phys. Chem. C*, 2007, **111**, 8849–8855.
41 K. Kim, H. S. Han, I. Choi, C. Lee, S. Hong, S.-H. Suh, L. P. Lee and T. Kang, *Nat. Commun.*, 2013, **4**, 2182.
42 M. P. Cecchini, V. A. Turek, J. Paget, A. A. Kornyshev and J. B. Edel, *Nat. Mater.*, 2012, **12**, 165–171.
43 G. Amarandei, C. O'Dwyer, A. Arshak and D. Corcoran, *ACS Appl. Mater. Interfaces*, 2013, **5**, 8655–8662.
44 K. Zhang, J. Zhao, J. Ji, Y. Li and B. Liu, *Anal. Chem.*, 2015, **87**, 8702–8708.
45 B.-L. Wang, M.-L. Ren, J.-F. Li and Z.-Y. Li, *J. Appl. Phys.*, 2012, **112**, 083102.
46 M. Hojeij, N. Younan, L. Ribeaucourt and H. H. Girault, *Nanoscale*, 2010, **2**, 1665–1669.
47 J. Butet, P.-F. Brevet and O. J. F. Martin, *ACS Nano*, 2015, **9**, 10545–10562.
48 E. Smirnov, P. Peljo, M. D. Scanlon and H. H. Girault, *Electrochim. Acta*, 2015, DOI: 10.1016/j.electacta.2015.10.104.
49 P. S. Toth, A. N. J. Rodgers, A. K. Rabiu and R. a. W. Dryfe, *Electrochem. Commun.*, 2015, **50**, 6–10.
50 J. Turkevich, P. C. Stevenson and J. Hillie, *Discuss. Faraday Soc.*, 1951, **11**, 75–82.
51 G. Frens, *Nat. Phys. Sci.*, 1973, **241**, 20.
52 W. Haiss, N. T. K. Thanh, J. Aveyard and D. G. Fernig, *Anal. Chem.*, 2007, **79**, 4215–4221.
53 M. Shopa, K. Kolwas, A. Derkachova and G. Derkachov, *Opto-Electron. Rev.*, 2010, **18**, 421–428.
54 A. B. Evlyukhin, C. Reinhardt, U. Zywietz and B. N. Chichkov, *Phys. Rev. B: Condens. Matter*, 2012, **85**, 245411.
55 V. Myroshnychenko, J. Rodríguez-Fernández, I. Pastoriza-Santos, A. M. Funston, C. Novo, P. Mulvaney, L. M. Liz-Marzán and F. J. García de Abajo, *Chem. Soc. Rev.*, 2008, **37**, 1792–1805.
56 H. Hinterwirth, S. K. Wiedmer, M. Moilanen, A. Lehner, G. Allmaier, T. Waitz, W. Lindner and M. Lämmerhofer, *J. Sep. Sci.*, 2013, **36**, 2952–2961.
57 S. Balog, L. Rodriguez-Lorenzo, C. A. Monnier, B. Michen, M. Obiols-Rabasa, L. Casal-Dujat, B. Rothen-Rutishauser, A. Petri-Fink and P. Schurtenberger, *J. Phys. Chem. C*, 2014, **118**, 17968–17974.
58 C. J. Sandroff, D. A. Weitz, J. C. Chung and D. R. Herschbach, *J. Phys. Chem.*, 1983, **87**, 2127–2133.
59 C. Novo, A. M. Funston, A. K. Gooding and P. Mulvaney, *J. Am. Chem. Soc.*, 2009, **131**, 14664–14666.
60 C. Novo, A. M. Funston and P. Mulvaney, *Nat. Nanotechnol.*, 2008, **3**, 598–602.
61 Z. Yang, S. Chen, P. Fang, B. Ren, H. H. Girault and Z. Tian, *Phys. Chem. Chem. Phys.*, 2013, **15**, 5374–5378.
62 M. Karg, N. Schelero, C. Oppel, M. Gradzielski, T. Hellweg and R. von Klitzing, *Chemistry*, 2011, **17**, 4648–4654.
63 M. Lista, D. Z. Liu and P. Mulvaney, *Langmuir*, 2014, **30**, 1932–1938.
64 Y. Liu, X. Han, L. He and Y. Yin, *Angew. Chem., Int. Ed.*, 2012, **51**, 6373–6377.
65 C. Goldmann, R. Lazzari, X. Paquez, C. Boissière, F. Ribot, C. Sanchez, C. Chanéac and D. Portehault, *ACS Nano*, 2015, **9**, 7572–7582.
66 H. Jung, H. Cha, D. Lee and S. Yoon, *ACS Nano*, 2015, **9**, 12292–12300.
67 N. Pazos-Perez, C. S. Wagner, J. M. Romo-Herrera, L. M. Liz-Marzán, F. J. García de Abajo, A. Wittemann, A. Fery and R. A. Alvarez-Puebla, *Angew. Chem., Int. Ed.*, 2012, **51**, 12688–12693.
68 D. Momotenko, *PhD Thesis*, EPFL, 2013.
69 H. Schwartz, Y. Harel and S. Efrima, *Langmuir*, 2001, **17**, 3884–3892.
70 R. Aveyard, J. H. Clint, D. Nees and N. Quirke, *Langmuir*, 2000, **16**, 8820–8828.
71 F. Bresme and M. Oettel, *J. Phys.: Condens. Matter*, 2007, **19**, 413101.
72 T. Atay, J.-H. Song and A. V. Nurmikko, *Nano Lett.*, 2004, **4**, 1627–1631.
73 M. P. Konrad, A. P. Doherty and S. E. J. Bell, *Anal. Chem.*, 2013, **85**, 6783–6789.
74 K. Zhang, J. Ji, Y. Li and B. Liu, *Anal. Chem.*, 2014, **86**, 6660–6665.
75 W. M. Haynes, *CRC Handbook of Chemistry & Physics*, Taylor & Francis Ltd, 95th edn, 2014.
76 M. Moskovits, I. Srnová-Šloufová and B. Vlčková, *J. Chem. Phys.*, 2002, **116**, 10435.

77 I. Srnová-Šloufová, F. Lednický, A. Gemperle and J. Gemperlová, *Langmuir*, 2000, **16**, 9928–9935.
78 Y. Zhuo, R. Yuan, Y. Chai, Y. Zhang, X. Li, N. Wang and Q. Zhu, *Sensors Actuators, B*, 2006, **114**, 631–639.
79 D. Liu, F. Zhou, C. Li, T. Zhang, H. Zhang, W. Cai and Y. Li, *Angew. Chem., Int. Ed.*, 2015, **54**, 9596–9600.
80 J. Wang, H. Busse, D. Syomin and B. E. Koel, *Surf. Sci.*, 2001, **494**, L741–L747.
81 J. Wang, B. A. Bansenauer and B. E. Koel, *Langmuir*, 1998, **14**, 3255–3263.
82 A. C. R. Pipino and V. Silin, *Chem. Phys. Lett.*, 2005, **404**, 361–364.
83 Z. Mao, H. Xu and D. Wang, *Adv. Funct. Mater.*, 2010, **20**, 1053–1074.
84 P. Huang, J. Lin, W. Li, P. Rong, Z. Wang, S. Wang, X. Wang, X. Sun, M. Aronova, G. Niu, R. D. Leapman, Z. Nie and X. Chen, *Angew. Chem., Int. Ed.*, 2013, **52**, 13958–13964.
85 J. Lin, S. Wang, P. Huang, Z. Wang, S. Chen, G. Niu, W. Li, J. He, D. Cui, G. Lu, X. Chen and Z. Nie, *ACS Nano*, 2013, **7**, 5320–5329.
86 K. Niikura, N. Iyo, Y. Matsuo, H. Mitomo and K. Ijiro, *ACS Appl. Mater. Interfaces*, 2013, **5**, 3900–3907.
87 J. Song, L. Pu, J. Zhou, B. Duan and H. Duan, *ACS Nano*, 2013, **7**, 9947–9960.